Solar Energy
And Sustainable Development
Refereed, biannual scientific journal issued by:
The Libyan Center for Solar Energy Research and Studies

Analysis of a Novel Coupled Inductor-Extended Double Stage Active Boost (CIX²AB) Converter Topology for Maximizing Output Efficiency in PV Power Systems

J. Viswanatha Rao[1*], J. Raji[2], M. Mohammadha Hussaini[3], G.W. Martin[4].

[1]Department of Electrical and Electronics Engineering, VNR Vignana Jyothi Institute of Engineering & Technology, Hyderabad, India.
[2]Department of Electrical and Electronics Engineering, Bharath Institute of Higher Education and Research, Chennai, India.
[3]Department of Electrical and Electronics Engineering, Government College of Engineering, Erode.
[4]Department of Electrical and Electronics Engineering, Marthandam College of Engineering and Technology, Tamilnadu, India.

E-mail: [1] viswanath72@gmail.com ,[2] jraji.bharath@gmail.com ,[3] hussaini1008@gmail.com ,[4] rgwmartinme@gmail.com .

ARTICLE INFO.

Article history:
Received 30 June 2025
Received in revised form 3 Jul 2025
Accepted 19 Aug 2025
Available online 26 Aug 2025

KEYWORDS

Renewable Energy Systems, Photovoltaic, CIX²AB Converter, Proportional Integral.

ABSTRACT

Solar energy is a critical aspect of Renewable Energy Systems (RES), driven by increasing cost-of-electricity and growing demand from utility customers for clean, pollution-free, sustainable energy. Distributed Photovoltaic (PV) generation systems generally produce low voltage, thus introducing a high step-up converter to interface efficiently with the load is crucial. Therefore, this paper provides a novel Coupled Inductor Extended Double Stage Active Boost (CIX²AB) Converter for enhancing voltage efficiency in PV system. Also, the Proportional Integral (PI) controller is utilized to regulate the converter and supports stabilization of output voltage. The numerical model of the CIX²AB converter circuit integrated with PV is implemented using MATLAB/Simulink software. The experimental verification demonstrates that the developed CIX²AB converter significantly contributes in achieving higher efficiency of 96.2% with enhanced voltage gain and reduced stress.

*Corresponding author.

DOI: https://doi.org/10.51646/jsesd.v14i2.643

تحليل مُحوّل مبتكر نشط ذو مرحلتين متصل مع محث مزدوج (CIX²AB) لتعزيز كفاءة الخرج في أنظمة الطاقة الكهروضوئية

ج. فيسواناثا راو، ج. راجي، م. محمد حسين، ج. مارتن.

ملخص: تُعَدُّ الطاقة الشمسية أكثر منظومات الطاقت المتجددة انتشارا، وذلك بسبب ارتفاع تكلفة الكهرباء وازدياد الطلب على الطاقة النظيفة والمستدامة. عادةً ما تُولِّد أنظمة الطاقة الكهروضوئية جهدًا منخفضًا، لذا فإن ربط محوّل رفع عالي الكفاءة مع الحمل يعد أمرا بالغ الأهمية. وبناءً عليه، يقدم هذا البحث مُحوِّلًا مبتكرًا سُمي بمُحوِّل الرفع النشط ذو المرحلتين المتصل مع محث مزدوج (CIX²AB) لتعزيز كفاءة الجهد في نظام الطاقة الكهروضوئية. وفي منظومات الكهروضوئية الأكبر حجمًا، يقوم هذا المحوّل المقترح برفع الجهد المستمر المنخفض الناتج من مصفوفة الألواح الشمسية إلى جهد أعلى وأكثر استقرارًا. كما تم الاستعانة بوحدة التحكم التناسبي التكاملي (PI) لتنظيم عمل المحوّل ودعم استقرار جهد الخرج. وقد تم تنفيذ النموذج العددي لدائرة محوّل CIX²AB المدمجة مع منظومة الاخلايا الشمسية باستخدام برنامج Simulink/MATLAB. وتُبيِّن النتائج أن المحّول CIX²AB يُسهم بشكل ملحوظ في تحقيق كفاءة عالية تصل إلى 96.2 % ورفع الجهد وتقليل الإجهاد.

الكلمات المفتاحية – منظومات الطاقة المتجددة، الطاقة الكهروضوئية، محوّل CIX²AB، وحدة التحكم التناسبي التكاملي.

1. INTRODUCTION

1.1. Background and Motivation Research

The fossil fuel depletion affects the automobile sector severely, due to environmental concerns, including global warming, the increased carbon footprint, etc [1]. Owing to the emissions of greenhouse gases and energy disaster, the generation of electrical power using fossil fuels is being replaced with RES around the world [2]. Currently, RES represents 25% of the world's capacity for power generation. Worldwide, population growth and environmental degradation are worsening due to higher fossil fuel consumption. The challenge of large distances transmitting electricity is driving the growing adoption of RES [3]. The growing use of Renewable Energy (RE) is mainly due to the pollution caused by fossil fuels [4]. Because RES are easy to maintain, environmentally friendly and highly efficient. The energy generation from a Solar Photovoltaic (SPV)-based RES decreases the energy crisis and ecological pollution [5].

The SPV structures are established in a series–parallel arrangement, for achieving high output voltage levels, which reduces their effectiveness and increases their overall size [6]. Yet, the shortfalls of SPV system include its dependency on output voltage load, limited power capacity, and reliance on environmental factors such as solar irradiation and temperature. These shortcomings are easily addressed with the combination of power converters [7]. However, due to the wide spectrum of RE and the variety of power converters presents challenges arise in effective implementation and integration [8]. The DC-DC converters are generally designed for a specific application and used across a range of power levels from low to high [9-10].

1.2. Literature Survey

B.M. Kiran Kumar et al (2021) [11] have developed Multiple Gain Boost Converter (MGBC) with Capacitor-Inductor-Capacitor (CLC) structure for integration of the SPV system for a grid. The MGBC is demonstrated to provide a huge improvement in boosting factor and allow for more voltage out of fewer components. However, owing to increase in number of components makes the system design more complex, results in higher cost and faces difficulties in implementation. Shima Sadaf et al (2021) [12] have introduced an active switched inductor network based high gain boost converter designed for DC application, provided high voltage gain and reduced number of components. The improved high gain switched inductor network reduced switch

voltage stress and conduction loss while also providing continuous input current. Nonetheless, addition of passive components increases the internal complexity. Mahnaz Izadi et al (2023) [13] have researched a non-isolated quadratic DC-DC boost converter achieving ultra-high voltage gain without need for a voltage doubler circuit while reduces voltage stress components, making it highly suitable for RE applications. Nevertheless, this system requires precise control and optimization to achieve stable operation within varying load condition. Sathish Ch. et al (2023) [14] have presented High Gain Modified Z-source Boost converter for addressing the low DC voltage and current produced by PV source. This contributes in limiting the number of power conversion stages, energy losses and better grid synchronization. However, the complexity of control system is increased, as it requires greater precise tuning to ensure stable and efficient operations. Seshagiri Rao et al (2022) [15] have developed a Voltage Multiplier Coupled Cascaded Boost Converter (VM-CBC) for solar PV applications in a DC microgrid to achieve greater voltage gain and efficiency. The VM-CBC affords continuous source current, better efficiencies and lower component stress with voltage and current yield performance. Nevertheless, this converter increased circuit complexity, creating higher power losses and an increased system impact. Table 1 provides a more overview of existing studies on DC-DC converters.

Table 1. Summary of exiting converter Performance.

Author name /Year	Converter	Operations	Limitations
Abualkasim Bakeer et al / 2022 [16]	Buck Boost	• Operates in buck and boost modes using phase shift modulation. • Transfers power from PV module to DC microgrid.	• Primary semiconductors are most vulnerable. • Trade-off between resonant tank parameters affects efficiency. • Reliability affected by PV mission profile variations.
V. Fernão pires et al /2021 [17]	Dual Output and High Voltage Gain DC-DC Converter	• Provides continuous input current and self-balancing outputs. • High voltage gain with reduced semiconductor voltage stress.	• Hard-switching operation may increase power losses. • Non-idealities in inductors limit voltage gain. • Parasitic elements affect dynamic response in practical implementations.
Mahajan Sagar Bhaskar et al / 2024 [18]	Scalable High-Voltage Gain Converter	• Converts lower DC voltage to higher DC voltage. • Scalable to multiple stages for increased voltage.	• Requires additional components for higher voltage gain. • Increased complexity with more stages. • Parasitic losses affect efficiency. • Component ratings impact cost and design
Davut Ertekin / 2022 [19]	High Gain Switched-inductor-capacitor DC-DC Boost Converter	• Minimizes input current ripples, improving PV panel efficiency. • Enhances energy extraction from PV sources.	• Requires additional components, increasing system complexity. • Voltage stress on diodes require specific component selection. • Efficiency decrease under certain load conditions.
Kanagaraj N et al /2024 [20]	High Boost Multi-Port Z-Network Converter	• Enhances voltage gain for better grid-tied PV applications. • Converts multiple input sources into a single DC bus.	• Struggle with low boost gain at high duty ratios. • High-frequency transformers increase design complexity and cost.

1.3. Contribution and Paper Organizarion

This paper proposes and investigates a novel CIX²AB converter topology for voltage boosting in PV applications. The key contributions of this paper are:

• The solar energy is transformed to DC electrical power by the PV system, which is supplied to the advanced CIX²AB converter.

• High gain voltage and efficiency are achieved in the CIX²AB converter by using coupled inductors and a two-stage boosting scheme.

• A PI controller is utilized for output voltage control in the PV system.

The article, section II explains the modelling of each of the system components, such as PV panel, converter, and controller. Section III presents the simulation results and a comparison of the converter performance based on voltage regulation and efficiency. Section IV summarizes the work by presenting the key findings and outlining future work directions.

2. PROPOSED SYSTEM METHODOLOGY

A PV system obtains voltage and current in the form of DC through the conversion of sunlight into electrical energy. However, the current and voltage produced by the PV system is low due to changing weather conditions from sunlight intensity, temperature, etc. This fluctuation makes regulating the output of PV panels necessary, thus a highly efficient DC-DC converter is utilized to provide a higher level output. The CIX²AB converter uses coupled inductance and utilizes a dual-stage design to increase the fluctuating PV voltage to a enhance DC output, minimizing loss and optimizing conversion efficiency as shown in Figure 1.

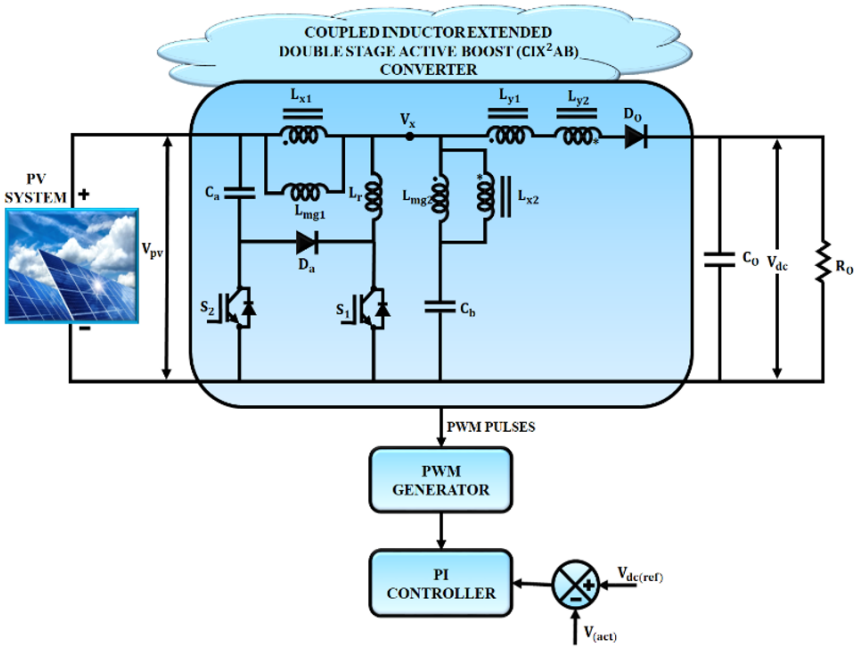

Figure 1. Proposed block diagram

The system employs a PI controller to generate a control signal for the PWM generator, which is produce switching pulses to control the converter. Each component work together to extract maximum power from PV maintaining stable, high-efficient performance characteristics against fluctuating environmental conditions to provide consistent power to the load.

2.1. PV system

A PV module is obtained by interconnecting a solar cell, a simple technology of converting

sunlight to pollution-free electricity. Similarly, these panels are linked in series and parallel to produce PV arrays, which produce green and clean energy. An individual solar cell is an element of an electrical circuit that includes a diode, a photocurrent generator, which is responsible for production of electricity from light. It also contains two resistors, one series and one parallel that signify the Joule effect and the recombined losses. The basic circuit design for a solar panel is depicted in Figure 2.

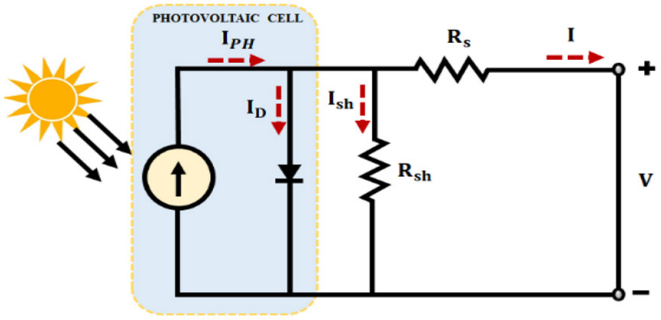

Figure 2. Basic Solar panel circuit.

Kirchhoff's law states that the PV cell's current operates as below:

$$I = I_{PH} - I_d - I_{sh} \qquad (1)$$

The shunt current expressed as:

$$I_{sh} = \frac{V + R_s I}{R_{sh}} = \frac{V_d}{R_{sh}} \qquad (2)$$

Here, I stands PV cell current output, I_{PH} and I_d represents photocurrent and diode current. I_{sh} and R_{sh} denotes shunt current and shunt resistance. V and R_s stands terminal voltage and series resistance respectively. Flowing of current over the diode defined as:

$$I_d = I_s \left(e^{\frac{V_d}{nV_t}} - 1 \right) \qquad (3)$$

The above formula, inverse saturation current and Ideality factor of diode denoted by I_s and n. V_t represents thermal voltage that written as:

$$V_t = \frac{N_s k T_c}{q} \qquad (4)$$

Here, k stands Boltzmann constant. q and N_s respectively represents electronic charge and number of cells linked in series. I_s is specified by subsequent calculation:

$$I_s = I_{sn} \left(\frac{T_c}{T_{ref}} \right)^3 e^{\left(\frac{E_{gO}\left(\frac{1}{T_n} - \frac{1}{T_c} \right)}{nk} \right)} \qquad (5)$$

The above calculation, I_{sn} denoted inverse saturation current at reference temperature assumed via expresses as:

$$I_{sn} = \frac{I_{CC}}{e^{\left(\frac{V_{co}}{nV_t} \right)} - 1} \qquad (6)$$

In this equation, I_{CC} and V_{co} represents short circuit current and open circuit voltage of PV cell.

Energy band gap of semiconductor denoted by E_{gO}. The I_{ph} calculated for any arbitrary value of G irradiance and T_c cell temperature by subsequent calculation:

$$I_{ph} = \frac{G}{G_{ref}} I_{cc} + k_i \left(T_c - T_{ref} \right) \quad (7)$$

Where, G_{ref} and . Tref represents reference irradiance and temperature. k_i stands temperature coefficient current. Thus the output current I of a PV system is defined as below:

$$I = I_{ph} - I_s \left(e^{\frac{V_d}{nV_t}} - 1 \right) - \frac{V_d}{R_{sh}} \quad (8)$$

A PV system is used to deliver energy to the load but the variability in changing environmental conditions, such as cloudy, raining significantly affect output voltage level. The proposed designed solution enhance the output voltage and maintain stability, through using a high-efficiency converter which is discussed below.

2.2. Coupled Inductor-Extended Double Stage Active Boost (Cix²Ab) Converter

A CIX²AB converter employed in a PV system that increase the voltage attained from PV panels. Coupled inductors enable high voltage gains and sufficient energy transfer, coupled with a double-stage boost topology, yield very high conversion ratios. The circuit as shown in Figure 3 includes coupled inductors (L_{x1}, L_{x2}, L_{mg1} , L_{mg2} , L_r), a switch (S_1, S_2), diodes (D_a , D_0), and capacitors (C_a ,C_b ,C_0). The converter operates in distinct modes defined by switch operation and energy transfer paths, which limit voltage stress, increase conversion ratio with a continuous input current for PV applications.

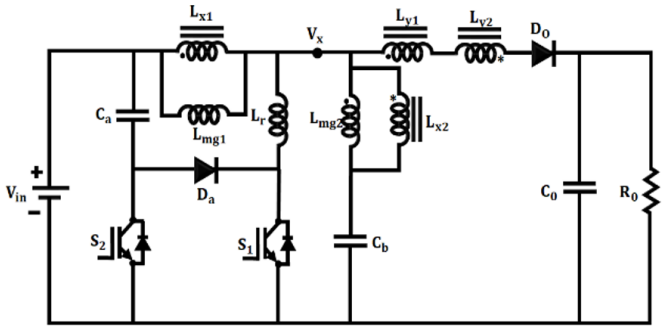

Figure 3. Proposed CIX²AB converter.

Mode 1:

Both switches, S_1 and S_2 are off in this mode shown in Figure 4 (a), which causes both switches to be off and enters into a freewheeling mode. At this point the energies stored in the magnetizing inductors, thus L_{mg1} and L_{mg2} are transferred to the load. The current flowing through the resonant inductor, L_r and the coupled inductors, L_{x1} and L_{x2} to help to boost the voltage. The capacitors, C_a and C_b are discharging their stored energies and continuing to provide continuous current to the output through diode, D_0. This mode is very short and only dependent on the resonance between the inductors and the capacitors, allowing decreased switching losses with increased efficiency from one mode to the other.

$$L_r \geq \frac{\left(C_{r1} + C_{r2} \right) \left[v_{DS1} \left(t_0 \right) \right]^2}{\left[i_{Lr} \left(t_0 \right) \right]^2} \quad (9)$$

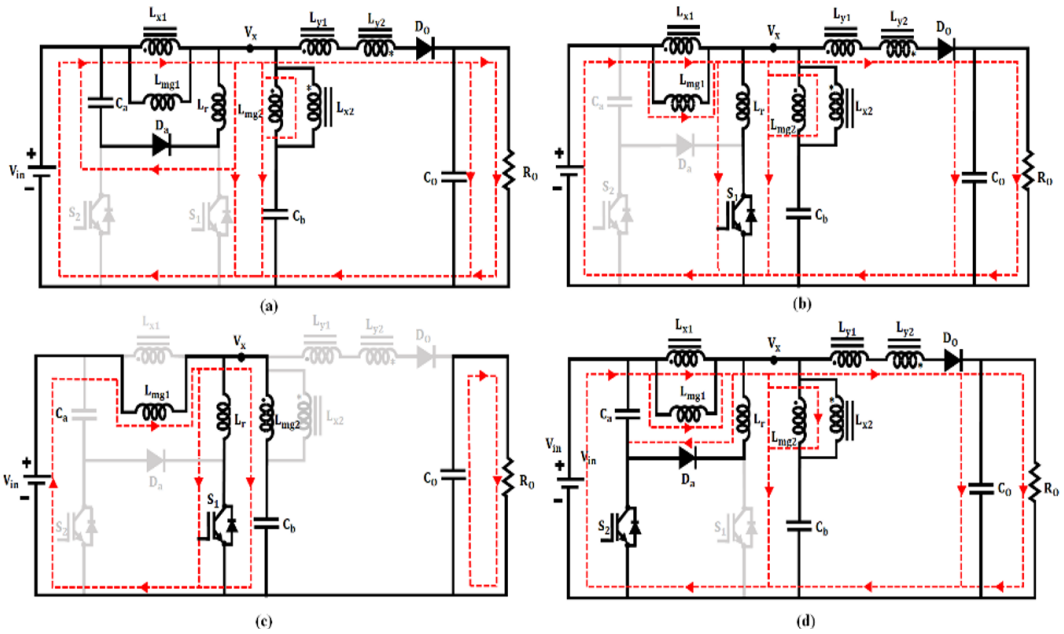

Figure 4. Modes of operations in proposed converter.

Mode 2:

In mode 2 shown in Figure 4 (b), switch S_2 is closed and current flow through the resonant inductor L_r . At this time, the combination of coupled inductors L_{x1} and L_{x2} , keep the load powered, while the output diode current i_{D0} is decreasing. The resonant current flows through L_r and reverses direction from negative to positive and grows until it reaches the combined magnetizing currents of i_{Lm1} and i_{Lm2} . In this active energy transfer step, magnetic coupling and interactions with the input-source determine the voltage at v_x and the voltages across the magnetizing inductors v_{Lmg1} and v_{Lmg2} .

$$v_x = \frac{2nV_{in} + V_o}{2n+1} \tag{10}$$

$$v_{Lmg1} = \frac{V_{in} - V_o}{2n+1} \tag{11}$$

$$v_{Lmg2} = \frac{-\left(V_{in} - V_o\right)}{2n+1} \tag{12}$$

The magnetizing inductor currents $i_{Lmg1}(t)$ and$i_{Lmg2}(t)$, resonant inductor current $i_{Lr}(t)$, and diode current $i_{Do}(t)$, written as:

$$i_{Lmg1}\left(t\right) = \frac{V_{in} - V_o}{\left(2n+1\right)L_{mg}}\left(t\right) + i_{Lmg1}\left(t_1\right) \tag{13}$$

$$i_{Lmg2}\left(t\right) = \frac{-\left(V_{in} - V_o\right)}{\left(2n+1\right)L_m g}\left(t\right) + i_{Lmg2}\left(t_1\right) \tag{14}$$

$$i_{Lr}\left(t\right) = \frac{2nV_{in} + v_o}{\left(2n+1\right)L_r}\left(t\right) + i_{Lr}\left(t_1\right) \tag{15}$$

$$i_{Do}\left(t\right) = \frac{i_{Lmg1}\left(t\right) - i_{Lmg2}\left(t\right) - i_{Lr}\left(t\right)}{2n+1} \tag{16}$$

Mode 3:

In Mode 3 shown in Figure 4 (c), switch S_1 is ON and is conducting the resonant inductor current i_{Lr} , equal to the total current of the magnetizing inductors i_{Lmg1} and i_{Lmg2} .
Switch S_2 is OFF, and energy delivered via input source is being supplied to both magnetizing inductors, where $v_{Lmg1} \approx V_{in}$ and $v_{Lmg2} \approx -V_{in}$ in to produce symmetry in the energy charging. During the mode, the output diode D_0 is in the reverse bias state, and the load is receiving power exclusively from the discharge of the output capacitor C_0. This mode ends once S_1 is turned OFF, and the node voltage v_x illustrates the dynamics of L_r , L_{mg1} , and L_{mg1} together.

$$v_x = V_{in}\frac{2L_r}{L_{mg}+2L_r} \tag{17}$$

$$v_{Lmg1} = V_{in}\frac{L_{mg}}{L_{mg}+2L_r} \tag{18}$$

$$v_{Lmg2} = -V_{in}\frac{L_{mg}}{L_{mg}+2L_r} \tag{19}$$

The magnetizing inductor currents i_{Lmg1}(t) and i_{Lmg2}(t), resonant inductor current $i_{Lr}(t)$, written as:

$$i_{Lmg1}\left(t\right) = \frac{V_{in}}{L_{mg}}\frac{L_{mg}}{L_{mg}+2L_r}t + i_{Lmg1}\left(t_2\right) \tag{20}$$

$$i_{Lmg2}\left(t\right) = \frac{V_{in}}{L_{mg}}\frac{-L_{mg}}{L_{mg}+2L_r}t + i_{Lmg2}\left(t_2\right) \tag{21}$$

$$i_{Lr}\left(t\right) = V_{in}\frac{2L_r}{L_m+2L_r}t + i_{Lr}\left(t_2\right) \tag{22}$$

Mode 4:

In Mode 4 shown in Figure 4 (d), switch S_2 is ON position and switch S_1 is OFF, allowing input voltage V_{in} to charge capacitor C_a and magnetize inductor L_{mg1} from the active path.
The auxiliary diode D_a became forward biased, allowing energy to be transferred from the primary side into the resonant network comprising L_r , L_{mg2} and capacitor C_b . Meanwhile, the coupled inductor assist with forwarding the increased energy through L_{y1} , and L_{y2} to the output through diode D_0 , which re-charges output capacitor C_0 and drives load R_0 . This mode allows efficient energy reusing and prepares the system for the subsequent switching cycle while keeping continuous conduction and large step-up gain.

$$v_x = \frac{2nV_{in}+V_o}{2n+1} \tag{23}$$

$$v_{Lmg1} = \frac{V_{in}-V_o}{2n+1} \tag{24}$$

$$v_{Lmg2} = \frac{-\left(V_{in}-V_o\right)}{2n+1} \tag{25}$$

The currents i_{Lmg1} , i_{Lmg2} , i_{Lr} and i_{Do} are written as:

$$i_{Lmg1}\left(t\right) = \frac{V_{in}-V_o}{\left(2n+1\right)L_{mg}}\left(t\right) + i_{Lmg1}\left(t_4\right) \tag{26}$$

$$i_{Lmg2}(t)=\frac{-(V_{in}-V_o)}{(2n+1)L_{mg}}(t)+i_{Lmg2}(t_4) \quad (27)$$

$$i_{Lr}(t)=\frac{2nV_{in}-v_o}{(2n+1)L_r}(t)+i_{Lr}(t_4) \quad (28)$$

$$i_{Do}(t)=\frac{i_{Lmg1}(t)-i_{Lmg2}(t)-i_{Lr}(t)}{2n+1} \quad (29)$$

Voltage transfer ratio:
The magnetising inductor L_{m1} volt-second balancing equation is:

$$\frac{V_{in}-V_0}{2n+1}D_{er}+V_{in}\frac{\frac{1}{2}L_{mg1}}{\frac{1}{2}L_{mg1}+L_r}(D-D_{er})+\frac{V_{in}-V_0}{2n+1}(1-D)=0 \quad (30)$$

Typically, magnetizing inductors L_{mg1} and L_{mg2} are larger than resonant inductors L_r. Equation (30) is reduced to Eq. (31) when the effects of duty loss D_{er} and resonant inductor L_r are disregarded, and then the ideal transfer function M_{ideal} is obtained as eq. (32).

$$V_{in}D+\frac{V_{in}-V_0}{2n+1}(1-D)=0 \quad (31)$$

$$M_{ideal}=\frac{2nD+1}{1-D} \quad (32)$$

Due to the effect of duty loss D_{er} , the voltage of the magnetizing inductor L_{mg1} fluctuates in duty cycle D. Equation (33) is redefined in light of the inductor's influence, and the transfer ratio $M=V_0/V_{in}$ in written as:

$$\frac{V_o}{V_{in}}=\frac{\frac{L_{mg}}{L_{mg}+2L_r}(D-D_{er})(2n+1)}{1-(D-D_{er})} \quad (33)$$

Duty loss D_{er} is obtained using equation (30) as follows:

$$D_{er}=\frac{-i_{Do_{Max}}(2n+1)}{T_s}\frac{1}{\left(\frac{v_{Lmg1}(A)}{L_{mg1}}-\frac{v_{Lmg2}(A)}{L_{mg2}}-\frac{v_{Lr}(A)}{L_r}\right)} \quad (34)$$

Here the diode's peak current is denoted i_{Do_Max} and the value obtained as:

$$i_{Do\_Max}=\frac{(1-D)T_s}{2n+1}\left(\frac{v_{Lmg1}(C)}{L_{mg1}}-\frac{v_{Lmg2}(C)}{L_{mg2}}-\frac{v_{Lr}(C)}{L_r}\right) \quad (35)$$

The I_o output current derived as:

$$I_o=\frac{i_{Do\_Max}}{2}\left[1-(D-D_{er})\right] \quad (36)$$

Figure 5 represents function of waveform of the proposed topology, divided into four paths in one cycle. The CIX²AB converter such as larger voltage gain, lower input current ripple, and lower

voltage stress on power switches making converter suitable to PV application. Coupled inductors provide a smaller form-factor as well as highly efficient energy transfers, mainly useful for step-up voltages applications containing high voltage ratios. Additionally, there is a PI controller in a PV system that regulates output voltage to minimize steady-state error, which is discussed below.

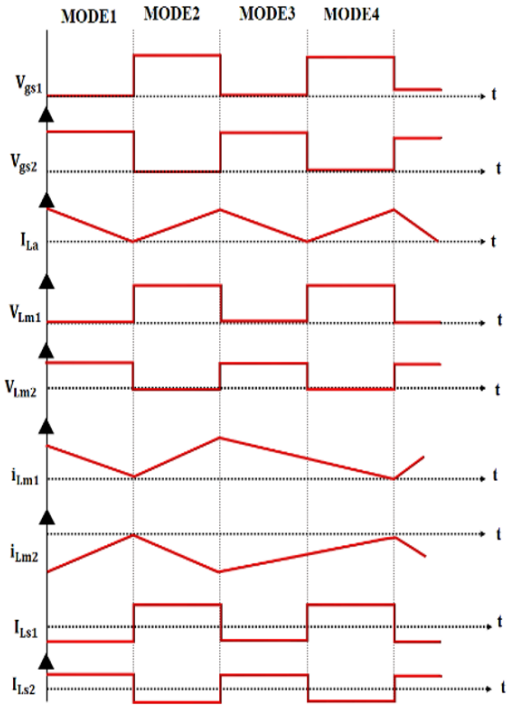

Figure 5. Key waveform of proposed converter.

2.3. PI Controller

A PI controller gradually regulates a control system that initially determines the fault, such as the difference between desired set point and current process parameter. The Proportional (P) component of controller multiplied the error via proportional gain (K_p) and performs a rapid action proportional to the error. The Integral (I) section analyses total amount of all preceding errors by integrating gain (K_i). The two modules P and I combine organised to calculate control output, which is subsequently used by the system as shown in Figure 6. This output affects the system's eventual output by reducing inaccuracy over time while maintaining the set point. Therefore, in this control signal is generated by summing error and integral of the error signal.

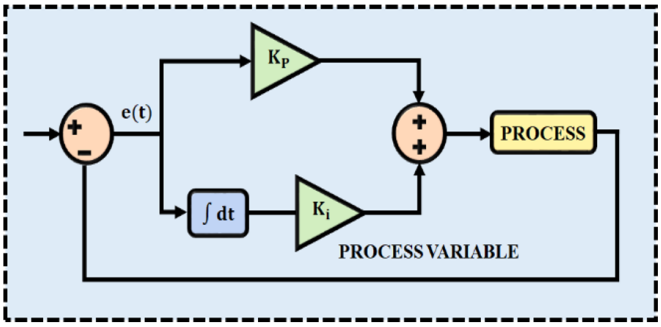

Figure 6. PI controller design.

$$m(t) = K_p e(t) + K_i \int e(t) \qquad (37)$$

Here, *m(t)* indicates controller output and *e(t)* signifies error signal. A PI controller is defined by the above formula, which adjusts output according to the present error and the total amount of previous errors. The Laplace transfer, the above-mentioned formula considered interpretation to obtain the controller's transfer function, which is provided as:

$$M(s) = K_p E(s) + K_i \frac{E(s)}{s} \quad (38)$$

Reducing common term, E(s) and obtain,

$$M(s) = E(s)\left[K_p + \frac{K_i}{s}\right] \quad (39)$$

It mentioned the error signal function as an input that causes the controller's output to change. Therefore on transferring E(s) to LHS, and obtain:

$$\frac{M(s)}{E(s)} = K_p + \frac{K_i}{s} \quad (40)$$

$$\frac{M(s)}{E(s)} = K_p\left[1 + \frac{K_i}{K_p s}\right] \quad (41)$$

$$\frac{M(s)}{E(s)} = K_p\left[1 + \frac{1}{T_i s}\right] \quad (42)$$

This calculation signifies the gain of PI controller.

$$T_i = K_p \,/\, K_i \quad (43)$$

The control system uses a PI controller to deliver a signal through a PWM generator, which makes the switching pulses that regulate the functioning of the converter. These above components work together to extract as much power as possible from the PV source, whilst also ensuring performance remains stable and efficient despite changing environmental factors to deliver consistent power to the load.

3. RESULT AND DISCUSSION

The proposed CIX²AB converter developed and tested in the MATLAB/Simulink environment. Three tests cases are used to determine its functionality including: steady-state, dynamic changing temperature and intensity, dynamic temperature with stable intensity cases. The results of the converters input and output responses are analysed for all cases, using the PI controller. Parameter specification details are presented in Table 2.

Table 2. Parameter Specifications.

Parameter	Specifications
PV System	
No. of panels connected in series	9
No. of panels connected in parallel	2
Rated Power	5kW
Open circuit voltage	37.25V
Short circuit current	8.95A
Remaining parameters	

CIX²AB Converter	
Switching Frequency	10kHz
L_{mg1} , L_{mg2} , L_{x1} , L_{x2} , L_{y1} , L_{y2} , L_r ,	4.7 mH
C_a , C_b	22µF
C_0	2200µF

Case 1: Steady State Condition of PV

Figure 7 describes the temperature and intensity waveforms of steady state condition on PV for case 1.

The first graph shows a temperature waveform indicating steady 35°C which means that the ambient thermal conditions for the PV had remained stable.

The intensity is shown constant around 900W/m², representing ideal irradiation for PV energy conversion.

It is established that the PV system at steady state operated under standard test conditions for Case 1 by the indicator values shown in both the temperature and intensity waveform.

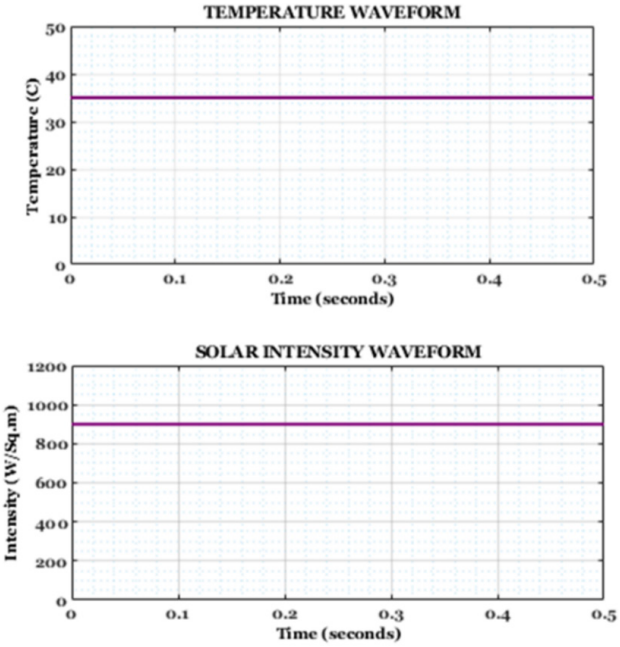

Figure 7. Waveform of temperature and intensity in steady state condition of PV.

Figure 8 illustrates the characteristics of CIX²AB converter during steady state condition.

The first waveform represents the steady DC voltage input of approximately 260 V.

This indicate that the PV solar power source supplying constant voltage power to the input. The second waveform represents the DC input current which shows slight transient and minor oscillations at the beginning, but its eventually stabilized with some oscillating ripples toward the end due to switching action and power balancing.

Figure 9 shows the output behavior of the CIX²AB converter controlled by a PI controller.

The first graph shows output voltage response of the converter.

The output voltage settles around 600 V after a transient response indicating that the voltage is well regulated. Next the output current waveform stabilizing at 9 A at beginning of the operation with minimal oscillations.

The results verify that the controlled output of PI controller is effective and the system is controllable for the steady state operation.

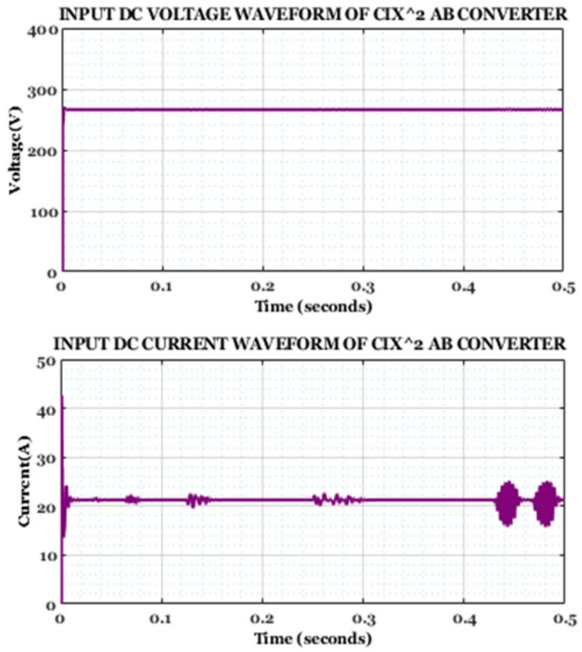

Figure 8. Waveform of input voltage and current in steady state condition of PV.

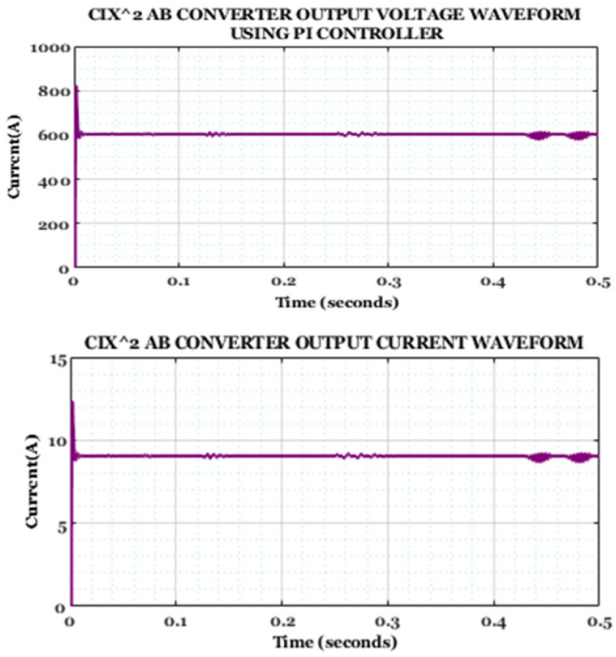

Figure 9. Waveforms of output voltage and current using CIX²AB converter with PI controller under steady state condition of PV.

Figure 10 presents the dynamic response of the PV system in Case 2 according to environmental conditions.

The first waveform shows the temperature increasing from approximately 27°C to 35 °C around 0.35 seconds, indicating a step of thermal change. The second waveform shows the solar intensity increasing from an approximate level of 900 W/m² to 1000 W/m² at the same time.

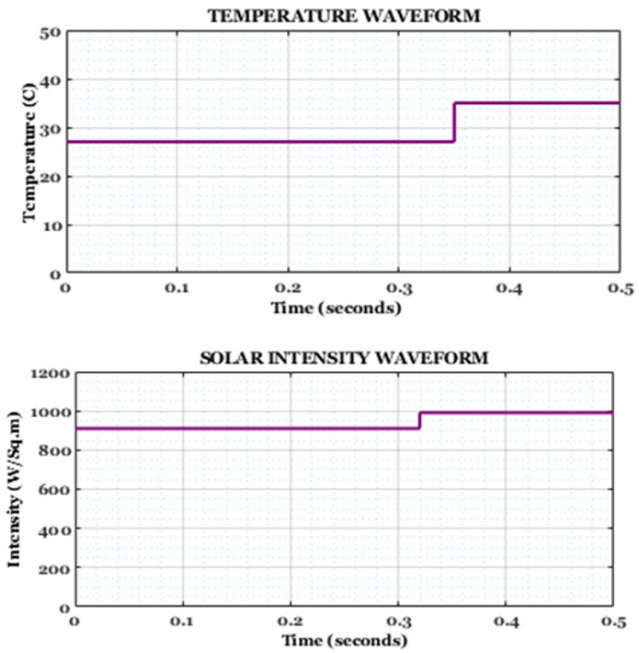

Figure 10. Temperature and intensity waveforms under varying condition in case 2 of PV system.

Case 2: Varying Condition of PV

Figure 11 displays environmental variations impacted the input features of the CIX²AB converter. The first image shows the input DC voltage, which started at a stable 260 V then decreased slightly, corresponding to the changing solar irradiance and temperature after 0.35 seconds. The second image shows the input current, which saw high fluctuations and some increased ripple after the disturbance, showing that the converter dynamically responding to the PV array's non-constant input power.

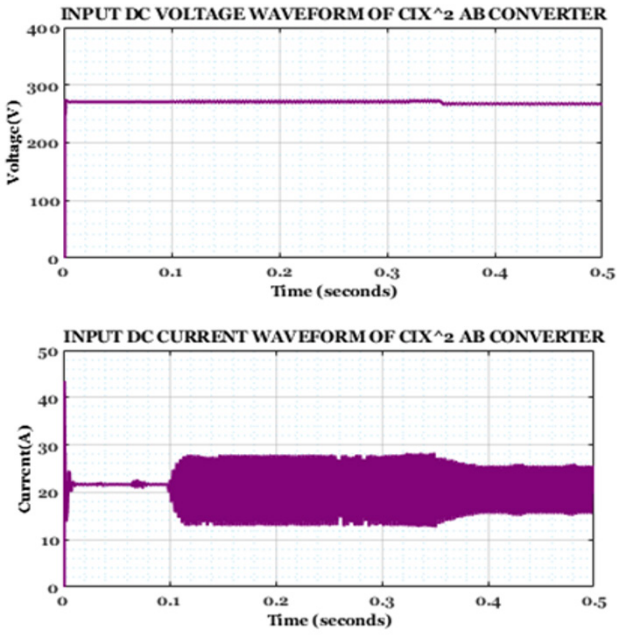

Figure 11. Input DC voltage and current waveform of the CIX²AB converter under varying condition of PV.

Figure 12 shows the output performance of the CIX²AB converter to different temperatures and solar irradiance. Despite variable conditions, the first waveform indicates that output voltage remained regulated in a 600 V region, while the second waveform shows that output current is

fairly stable at approximately 9 A. The results from the PI controller and the converter maintains steady voltage and current output during variations in temperature and solar intensity.

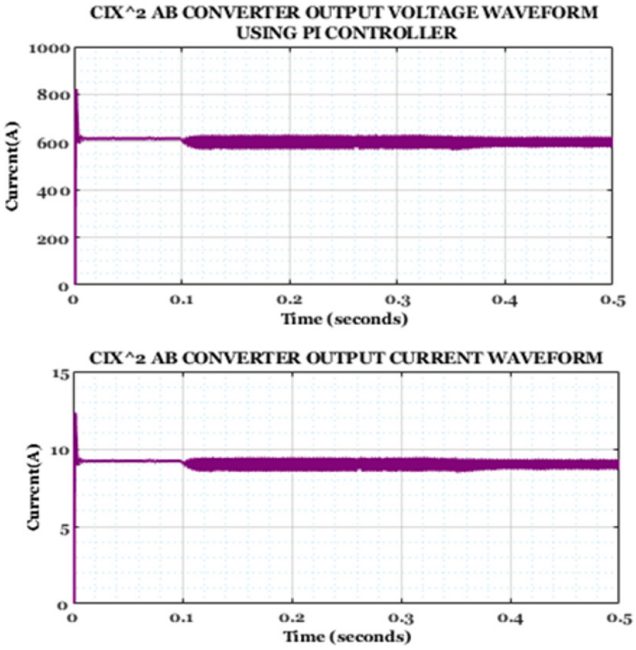

Figure 12. CIX²AB converter output voltage and current waveform using PI controller under varying condition of PV.

Case 3: Varying Temperature and Constant Irradiation

Figure 13 illustrates the environmental conditions of the PV system under Case 3. As seen in the first image, the temperature rises from about 25 °C to 33 °C around 0.35 seconds, simulating a stepped change in temperature. The second image shows constant intensity of 950 W/m² maintained throughout the test duration. The test case 3 evaluates the converter's performance during rapid temperature changes while maintaining constant solar irradiance.

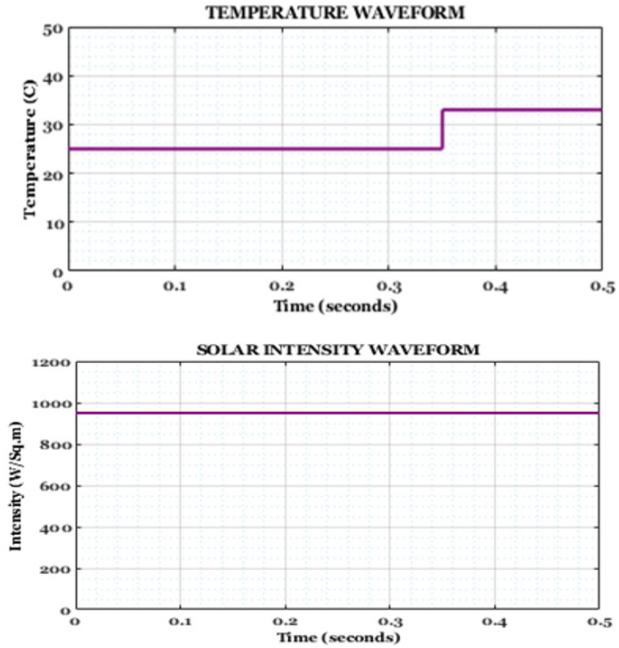

Figure13. Waveform of varying temperature and constant irradiation of PV.

Figure 14 shows input response of the converter when a temperature rise occurs in the PV system under constant irradiance conditions. The first waveform shows that the input voltage relatively steady at around 260 V, with drop occurring after 0.35 seconds which corresponded with the temperature increase. The input current varies significantly in the second waveform and stabilizes shortly, with some noticeable ripples at the beginning. These results show that the converter effectively manages temperature changes, maintaining voltage stability and rapidly adjusting input current despite initial instabilities.

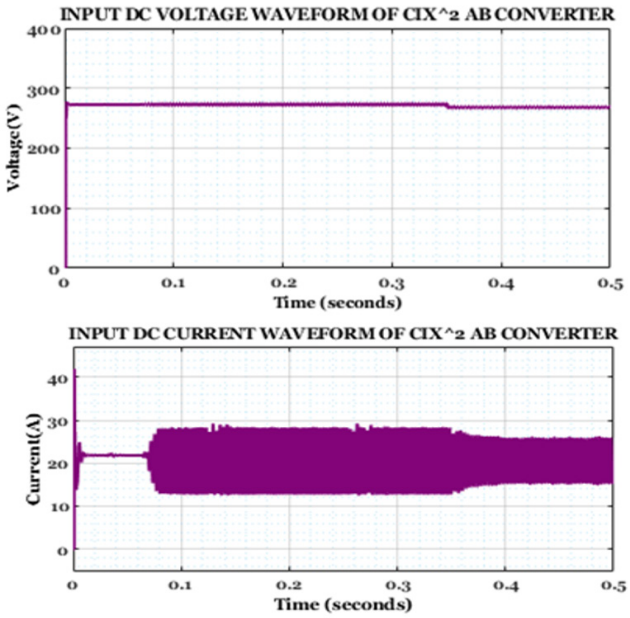

Figure 14. Input voltage and current waveform of CIX²AB converter in case 3.

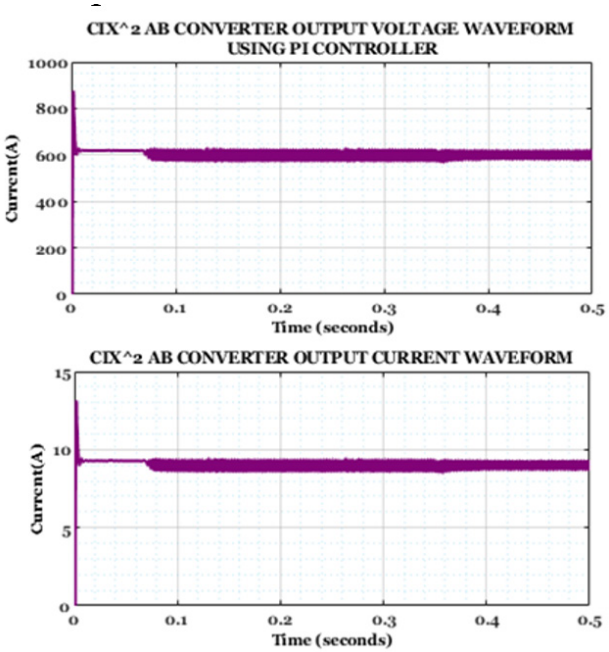

Figure 15. Output voltage and current waveform of CIX²AB converter in case 3.

Figure 15 shows regulated output of the CIX²AB converter as a function of temperature increase. The first image shows that the output voltage stabilizes around 600 V, and second image shows that the output current to stays around 9 A with small ripple. These results validate the converter's

capability to retain output stability even under changing thermal conditions, demonstrating effective performance of the control strategy.

Comparison:

The proposed CIX²AB converter compares to various existing converter topologies, including Double Boost Converter [21], Single Input Multi-Output Converter [22], Dual Switch Non-Isolated High Gain Converter [23], High Gain Boost Converter [24], Switch-LC-Based DC-DC Converter [25], and Non-Isolated Quadratic Boost Converter [26]. The evaluation primarily established on the efficiency, voltage gain, voltage stress on diode and switching devices.

Figure 16 represents the proposed converter delivers the highest efficiency of 96.2%, which is significantly better than other listed converter. The results specify that the proposed converter design achieves better performance due to reduced conduction losses, reduced switching losses, and improvement in energy transfer characteristics.

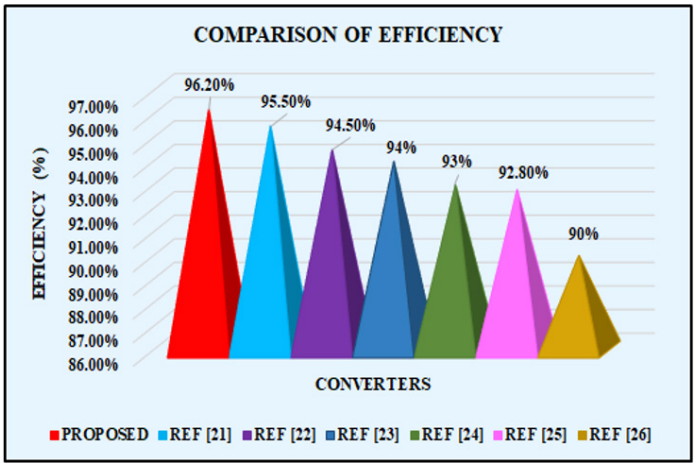

Figure 16. Comparison of efficiency in various converter.

The voltage gain characteristics in Figure 17 shows that throughout the range of duty cycles, the proposed converter delivers greater gain than other listed converters. At the moderate to high duty cycle region, the proposed converter delivers much more voltage gain than the existing converters. Also, the proposed topology is highly favourable for applications requiring high step-up voltage conversion.

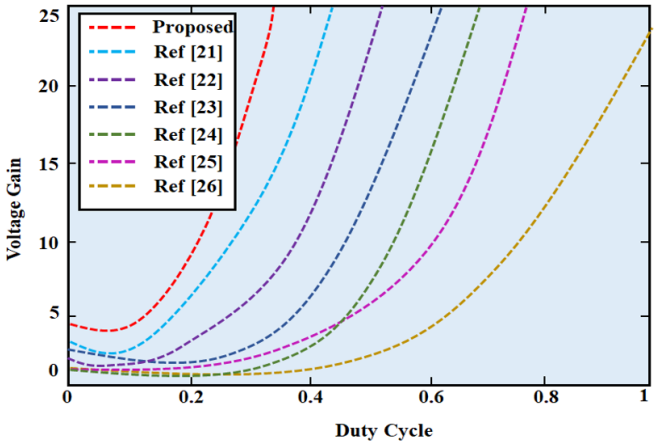

Figure 17. Comparison of voltage gain.

The normalized stress on switch and diode is represented in Figure 18 comparing the proposed method with other existing methods. As indicated in the comparison, the proposed method

shows less voltage stress on both switch and diode. The proposed CIX²AB converter has much lower and rapidly increasing voltage stress, while existing methods have significantly greater and rapidly increasing voltage stress as the voltage gain is increased. It demonstrates the proposed converter's superiority in terms of performance and component stress, as well as delivering enhanced efficiency in high-gain application.

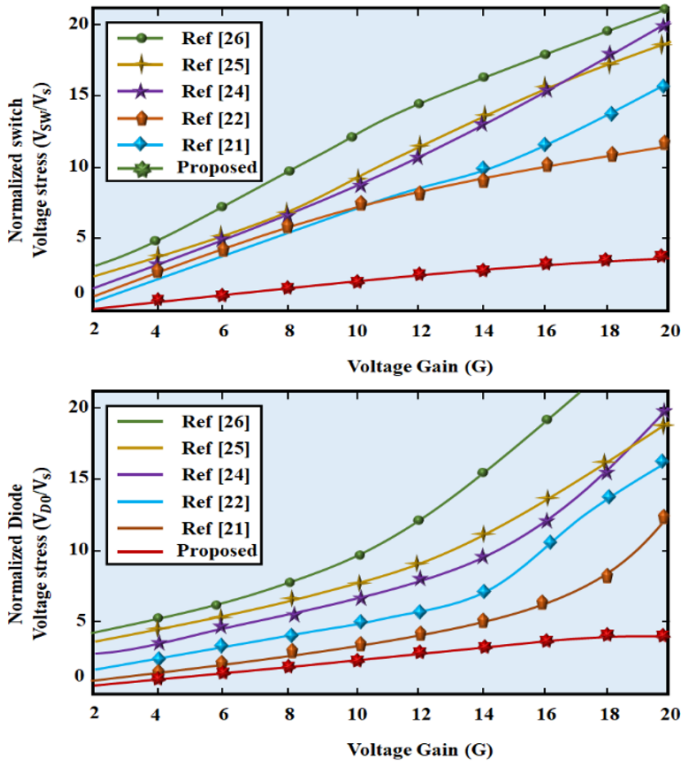

Figure 18. Comparison of voltage stress.

4. CONCLUSION

The proposed CIX²AB converter design signifies an effective and practical solution of enhancing the voltage output and successfully extract the maximum power from PV systems. Also, the converter achieves dynamic regulation and a stability in operation with loads and changing solar irradiance through the use of PI controller. The results from case simulation and experimentation indicates the developed CIX²AB converter achieves a high efficiency of 96.2%, achieving greater voltage gain with less switching losses. This novel architecture achieves efficient, consistent and scalable methodology for future enhanced performance solar energy applications, and is ideally situated for contemporary distributed generation systems and networks with future prospective.

Author Contributions: Conceptualization: J. Viswanatha Rao; Data Curation: J. Viswanatha Rao; Methodology: J. Raji, M. Mohammadha Hussaini, G.W. Martin & J. Viswanatha Rao; Project administration: J. Raji, M. Mohammadha Hussaini, G.W. Martin; Supervision: J. Raji, M. Mohammadha Hussaini, G.W. Martin; Validation J. Raji, M. Mohammadha Hussaini, G.W. Martin; Writing-original draft: J. Viswanatha Rao; Writing-review & editing: J. Raji, M. Mohammadha Hussaini, G.W. Martin & J. Viswanatha Rao.

Funding: This research received no external funding.

Data Availability: The data are available at request.

Conflicts of Interest: The authors declare that they have no conflict of interest.

REFERENCES

[1] M. J. Sathik, M. F. Elmorshedy, and D. J. Almakhles, "A New Boost Topology Seven-Level Inverter of High Voltage Gain Ability and Continuous Input Current with MPPT for PV Grid Integration", IEEE Access, vol. 11, pp. 139236-139248, Dec. 2023.

[2] P. K. Chamarthi, A. Al-Durra, T. H. El-Fouly, and K. A. Jaafari, "A novel three-phase transformerless cascaded multilevel inverter topology for grid-connected solar PV applications", IEEE Transactions on Industry Applications, vol. 57, no. 3, pp. 2285-2297, Feb. 2021.

[3] K. S. Kavin, P. S. Karuvelam, M. D. Raj, and M. Sivasubramanian, "A novel KSK converter with machine learning MPPT for PV applications", Electric Power Components and Systems, pp. 1-19, Apr. 2024.

[4] X. Fang, Q. Yang, and W. Yan, "Power generation maximization of distributed photovoltaic systems using dynamic topology reconfiguration", Protection and Control of Modern Power Systems, vol. 7, no. 3, pp. 1-15, Jul. 2022.

[5] Veerabhadra, and S. N. Rao, "Assessment of high-gain quadratic boost converter with hybrid-based maximum power point tracking technique for solar photovoltaic systems", Clean Energy, vol. 6, no. 4, pp. 632-645, Aug. 2022.

[6] K. S. Kavin, P. S. Karuvelam, M. Matcha, and S. Vendoti, "Improved BRBFNN-based MPPT algorithm for coupled inductor KSK converter for sustainable PV system applications", Electrical Engineering, pp. 1-23, Jan. 2025.

[7] M. Dhananjaya, D. Potnuru, P. Manoharan, and H. H. Alhelou, "Design and implementation of single-input-multi-output DC-DC converter topology for auxiliary power modules of electric vehicle", IEEE Access, vol. 10, pp. 76975-76989, Jul. 2022.

[8] M. Z. Malik, H. M. Farh, A. M. Al-Shaalan, A. A. Al-Shamma'a, and H. H. Alhelou, "A novel single-input-multi-output converter for flexible-order power-distributive with MPPT capability", IEEE Access, vol. 9, pp. 131020-131032, Sep. 2021.

[9] M. I. Marei, B. N. Alajmi, I. Abdelsalam, and N. A. Ahmed, "An integrated topology of three-port DC-DC converter for PV-battery power systems", IEEE Open Journal of the Industrial Electronics Society, vol. 3, pp. 409-419, Jun. 2022.

[10] C. H. Lin, M. S. Khan, J. Ahmad, H. D. Liu, and T. C. Hsiao, "Design and analysis of novel high-gain boost converter for renewable energy systems (RES)", IEEE access, vol. 12, pp. 24262-24273, Feb. 2024.

[11] B. M. Kiran Kumar, M. S. Indira, and S. N. Rao, "Performance analysis of multiple gain boost converter with hybrid maximum power point tracker for solar PV connected to grid", Clean Energy, vol. 5, no. 4, pp. 655-672, Dec. 2021.

[12] S. Sadaf, N. Al-Emadi, P. K. Maroti, and A. Iqbal, "A new high gain active switched network-based boost converter for DC microgrid application", IEEE Access, vol. 9, pp. 68253-68265, May. 2021.

[13] M. Izadi, A. Mosallanejad, and A. L. Eshkevari, "A non-isolated quadratic boost converter with improved gain, high efficiency, and continuous input current", IET Power Electronics, vol. 16, no. 2, pp. 193-208, Feb. 2023.

[14] S. Ch, I. A. Chidambaram, and M. Manikandan, "Hybrid Renewable Energy System with High Gain Modified Z-Source Boost Converter for Grid-Tied Applications", vol. 1, no. 57, pp. 39-54, Mar. 2023.

[15] V. S. Rao, and K. Sundaramoorthy, "Performance analysis of voltage multiplier coupled

cascaded boost converter with solar PV integration for DC microgrid application", IEEE Transactions on Industry Applications, vol. 59, no. 1, pp. 1013-1023, Sep. 2022.

[16] A. Bakeer, A. Chub, and Y. Shen, "Reliability evaluation of isolated buck-boost DC-DC series resonant converter", IEEE Open Journal of Power Electronics, vol. 3, pp. 131-141, Mar. 2022.

[17] V. F. Pires, A. Cordeiro, D. Foito, and J. F. A. Silva, "Dual output and high voltage gain DC-DC converter for PV and fuel cell generators connected to DC bipolar microgrids", IEEE Access, vol. 9, pp. 157124-157133, Oct. 2021.

[18] M. S. Bhaskar, S. R. Vemparala, D. Almakhles, S. K. and M. F. Elmorshedy, "A Scalable High-Voltage Gain DC/DC Converter with Reduced Voltage Stress for DC Microgrid Integration", IEEE Open Journal of the Industrial Electronics Society, Jan. 2025.

[19] D. Ertekin, "A high gain switched-inductor-capacitor DC-DC boost conveter for photovoltaic-based micro-grid applications", CSEE Journal of Power and Energy Systems, Sep. 2023.

[20] N. Kanagaraj, M. Ramasamy, and M. Vijayakumar, "Design of an extendable high boost multi-port Z-network converter for small power grid-connected PV applications", IEEE Open Journal of Power Electronics, vol. 5, pp. 534-553, Apr. 2024.

[21] H. Li, L. Zhu, and L. Wang, "A Double-Boost Converter Based on Coupled Inductance and Magnetic Integration", Active and Passive Electronic Components, vol. 2021, no. 1, pp. 8014620, 2021.

[22] M. Z. Malik, H. M. Farh, A. M. Al-Shaalan, A. A. Al-Shamma'a, and H. H. Alhelou, "A novel single-input-multi-output converter for flexible-order power-distributive with MPPT capability", IEEE Access, vol. 9, pp. 131020-131032, Sep. 2021.

[23] S. Khan, A. Mahmood, M. Tariq, M. Zaid, I. Khan, and S. Rahman, "Improved dual switch non-isolated high gain boost converter for DC microgrid application", In 2021 IEEE Texas Power and Energy Conference (TPEC), pp. 1-6, Feb. 2021.

[24] A. S. Mansour, A. H. H. Amer, E. E. El-Kholy, and M. S. Zaky, "High gain DC/DC converter with continuous input current for renewable energy applications", Scientific Reports, vol. 12, no. 1, pp. 12138, Jul. 2022.

[25] A. Kumar, Y. Wang, X. Pan, M. Raghuram, S. K. Singh, X. Xiong, and A. K. Tripathi, "Switched-LC based high gain converter with lower component count", IEEE transactions on industry applications, vol. 56, no. 3, pp. 2816-2827, Mar. 2020.

[26] N. Subhani, Z. May, M. K. Alam, I. Khan, M. A. Hossain, and S. Mamun, "An improved non-isolated quadratic DC-DC boost converter with ultra-high gain ability", IEEE Access, vol. 11, pp. 11350-11363, Feb. 2023.